Force Sensor Design and Measurement for Endodontic Therapy

Chih-Chiang Tsao, Fang-Yu Lin, Ji-Wei Liou, Ping-Han Wen, Chieh-Chung Peng, and Tzong-Shi Liu

***Abstract*— To assist endodontic therapy, in this paper, a force sensor is designed and fabricated for measuring the axial force and the bending moment simultaneously. By detecting the bending moment, we can know the severity of bending. Axial force detection is also desired, as excessive axial forces may result in instrument buckling or even root canal perforation. This paper installs three sensing cells in each of two planes to detect the bending direction. Each sensing cell consists of a pressure-sensitive electric conductive rubber and an electrode. The size of the force sensor is 1.4-mm wide and 6-mm high for matching the size of endodontic instruments and making it feasible in the endodontic treatment. Experimental results on accuracy, repeatability, and nonlinearity are presented to validate the proposed sensor.**

***Index Terms*— Force sensor, endodontic therapy, piezoresistive, bending sensing.**

I. Introduction

ENDODONTIC therapy is a common dental surgery. According to statistics, almost 28% of files were fractured after normal use from dentists [1]. Moreover, broken endodontic instruments in root canal may cause problem, and it causes anxiety and frustration for experienced dentists when trying to remove this fragment [2]. Therefore, any kind of fracture of rotary instruments is concerned by dentists. Fatigue life tests of rotary instruments were presented for predicting break [3]–[5]. It shows that the lifetime of endodontic instruments is about hundreds of cycles that depend on the size of instruments and the degree of bending.

The canal geometry and curvature can be evaluated before root canal treatment by using X-ray radiography [6]. However, the radiograph may not reflect the curvature correctly and cannot keep monitoring during therapy. An endodontic rotary instrument was combined with an in situ curvature sensor [7], which was based on the leakage of light energy from a flexible optical fiber with a constricted core. The curvature sensor can directly measure the bending of a file, but the sensing range of root canal curvature is limited. A force testing system [8] was proposed to measure the apical force and torque during preparation of curved canals by using a torque sensor and a force transducer. Although the system is complete, the sensing system is too large for clinical surgery.

The fatigue failure criterion of Goodman [9], takes into account the mean stress σ_m and stress amplitude σ_a

$$\frac{\sigma_a}{\sigma_{am}} + \frac{\sigma_m}{\sigma_u} = 1 \tag{1}$$

where σ_{am} is the fatigue strength with zero mean stress, and σ_u is the ultimate strength. Therefore, both the bending moments and axial forces influence NiTi instrument fatigue life. And because it is lack of complete force monitoring method in today root canal treatment, a force sensor with a miniature size is designed and fabricated in this paper for simultaneously measuring axial forces and bending moments. The advantage of simultaneous monitoring the axial force and the bending moment lies in obtaining a complete force sensing system to avoid fatigue failure and surgical errors. In addition, simultaneous sensing axial forces and bending moments can minimize the volume of the sensor and make it feasible. By knowing the bending moment of the instrument, one not only can obtain instrument deformation but also predict fatigue life of the instrument and make sure that the current feed direction is appropriate. Axial forces were affected by both canal type and preparation stage [8]. Excessive axial forces may result in instrument buckling or even root canal perforation. This paper installs three sensing cells in each of two planes. Each sensing cell is made of pressure-sensitive electric conductive rubber. This kind of rubber has been used to calculate the magnitude and the distribution of skin pressure [10], and we usually use it as a tactile sensor. It can detect the contact force between two contact surfaces. Hence, it was used as a force-feedback sensor in robots for measuring clamping forces between two moving parts [11]. Traditionally, a tactile sensor is limited to 1-D measurement, but a 3-D tactile sensor for measuring triaxial force without a complex structure has been realized [12]. For endodontic therapy, this paper aims at developing a sensor to sense the axial force and the bending moment simultaneously.

Manuscript received February 6, 2013; revised March 26, 2013; accepted April 2, 2013. Date of publication April 15, 2013; date of current version May 29, 2013. This work was supported in part by Mackay Memorial Hospital, the "Aiming for the Top University Program" of National Chiao Tung University and Ministry of Education, Taiwan. The associate editor coordinating the review of this paper and approving it for publication was Prof. Boris Stoeber.

C.-C. Tsao and T.-S. Liu are with the Department of Mechanical Engineering, National Chiao Tung University, Hsinchu 30010, Taiwan (e-mail: t102229a.me97g@g2.nctu.edu.tw; tsliu@mail.nctu.edu.tw).

F.-Y. Lin was with the Department of Mechanical Engineering, National Chiao Tung University, Hsinchu 30010, Taiwan. He is now with the Department of Electrical Engineering at National Taiwan University, Taipei 10617, Taiwan (e-mail: hoga85@gmail.com).

J.-W. Liou and C.-C. Peng are with the Division of Endodontics, Department of Dentistry, Mackay Memorial Hospital, Taipei 10449, Taiwan (e-mail: a4716@ms7.mmh.org.tw; ashken.peng@msa.hinet.net).

P.-H. Wen was with the Division of Endodontics, Department of Dentistry, Mackay Memorial Hospital, Taipei 10449, Taiwan. He is now with the Chengan Dental Clinic, Taipei, Taiwan (e-mail: bernardwen65@yahoo.com.tw).

Color versions of one or more of the figures in this paper are available online at http://ieeexplore.ieee.org.

Digital Object Identifier 10.1109/JSEN.2013.2258151

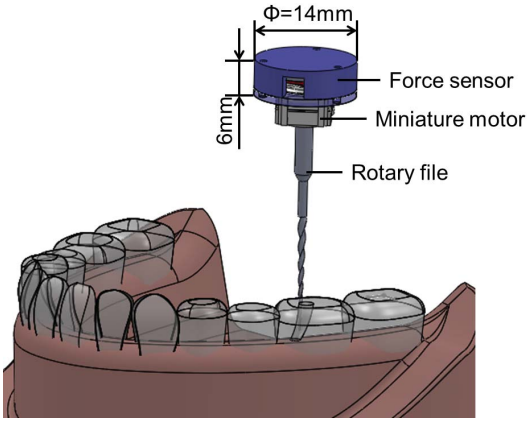

Fig. 1. Schematic diagram of the force sensor attached to a miniature motor and a rotary instrument for endodontic therapy.

II. Materials and Methods

A. Sensing Material

Piezoresistive materials can be used to sense forces. A type of polymer thick film is used as sensing material which is manufactured by Interlink Electronics, USA. It exhibits a decrease in resistance with an increase in the normal force applied to the surface. When the load is larger than 0.2 N, the relationship between the force and the resistance is linear [13]. The material appearance is in black flexible sheet form, 0.3 mm in thickness. It can be glued onto the surface of pectinate electrodes. The characteristic parameters [13] include: sensitivity of 0.21 kΩ/N, repeatability of 2% rate output, stability of lower than 5% full scale after 10 days, resolution of 0.5% full scale, and operation temperature range of −30 °C to 70 °C [13]. The performance of the sensing material is affected by environmental temperature. The typical resistance will be respectively decreased by 5% and 15% under −40 °C and 85 °C environmental temperature and the sensing material will be damageable when the environmental temperature is over 215 °C [13]. The pressure and force capacities of the sensing material are 98.1 N/cm^2 and 98.1 N [13], respectively. Under the maximum load limit, the lifetime of the sensing material is over 10 million actuations [13]. Moreover, the material will start to deform plastically around 688 N/cm^2 [13]. This paper adopts piezoresistive materials for the six sensing cells in the sensor. Since the material can sense forces or pressures directly, unlike strain gauges we do not have to sense the strain first and in turn use the strain to calculate the force. Hence, using piezoresistive materials saves the sensor volume.

B. Sensor Layout and Principle

The schematic diagram of the proposed force sensor is shown in Fig. 1. The force sensor with 14 mm diameter and 6 mm height is attached to a miniature motor and a rotary instrument. The miniature motor will supply the power source for drilling.

As shown in Fig. 2, the force sensor consists of a top housing, a core, and a bottom housing. The top housing and the bottom housing are screwed together via three bolted holes.

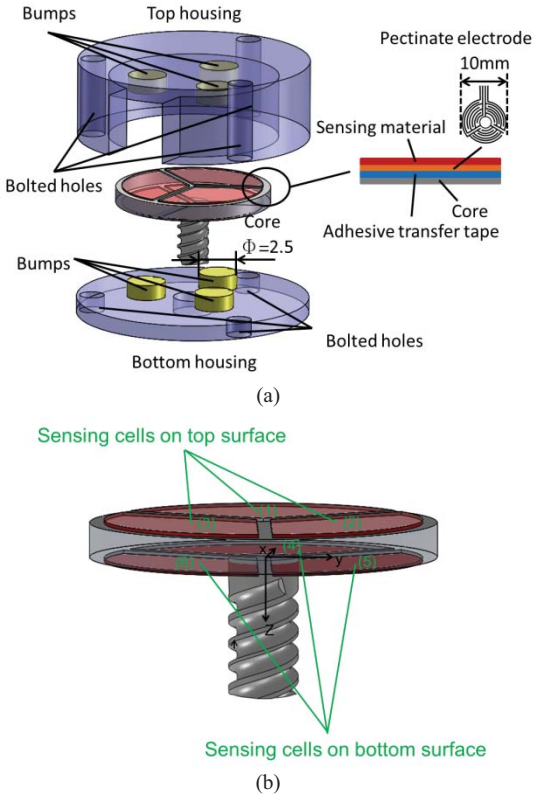

Fig. 2. (a) Structure of the sensor including the top housing, the core, and the bottom housing. (b) Three sensing cells on the top and bottom surfaces.

This design uses six sensing cells pasted on the core surfaces. Each sensing cell consists of a pressure-sensitive electric conductive rubber and a pectinate electrode film. Pectinate electrode films with 10 mm diameter are attached to the core by two adhesive transfer tapes. The pressure-sensitive electric conductive rubber is glued to the pectinate electrode. A bottom housing and a top housing respectively contain three bumps made of iron to make contact forces act on sensing cells. Each bump has 2.5 mm diameter; therefore, the capacity of each sensing cell is about 4.8 N. The shape of the sensing cells is a one-third circular plate of common diameter. Therefore, three sensing cells together become a circle.

When a file is pushed to enter a curved and narrow root canal, the curvature of the file will fit the root canal. The file is subjected to forces and moments in the curved root canal. As depicted in Fig. 3, the bending moment $\vec{M}$ caused by both couple and lateral force can be decomposed into x-component $\vec{M}_x$ and y-component $\vec{M}_y$. In addition, the friction force is the feeding resistance that causes an axial force $\vec{F}$ on the device. The lateral force causes the reaction force on the core from the top housing and can not be measured by using the present sensor. Fig. 3 shows that sensing cells on the bottom surface are used to sense the upward force, while sensing cells on the top surface are used to sense the downward force. Sensors are installed on both surfaces rather than single surface, because piezoresistive materials used in this paper can sense compressive forces but not tensile forces. $\vec{F}_i$, $i = 1, 2, 3, 4, 5, 6$ represent forces acting on six sensing cells come from bumps attached to housings and are converted

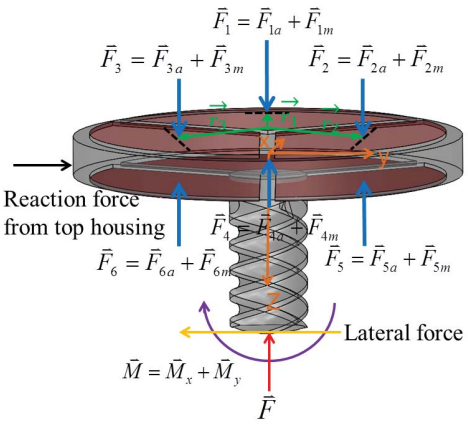

Fig. 3. Force $\vec{F}$ and moment $\vec{M}$ acting on the instrument result in three forces $\vec{F}_i$, $i = 1$, 2, and 3 applied to top three sensing cells and three forces $\vec{F}_i$, $i = 4$, 5, and 6 to the bottom three sensing cells. Resulting from force $\vec{F}$, $\vec{F}_{ia}$, $i = 1$–6 are contact forces between sensing cells and bumps, while resulting from moment $\vec{M}$, $\vec{F}_{im}$, $i = 1$–6 are contact forces between sensing cells and bumps.

to electric voltage in measurement. $\vec{r}_i$, $i = 1, 2, 3, 4, 5, 6$ are the radius vectors of $\vec{F}_i$ from the center of the core. Sensing cells on both surfaces are symmetric with respect to each other. Thus, $\vec{r}_1$ is equal to $\vec{r}_4$, $\vec{r}_2$ is equal to $\vec{r}_5$ and $\vec{r}_3$ is equal to $\vec{r}_6$. Moreover, since the forces acting the sensing cells result from both the axial force and the bending moment as shown in Fig. 3, the forces can be expressed by both axial and bending components

$$\vec{F}_1 = \vec{F}_{1a} + \vec{F}_{1m} \tag{2}$$
$$\vec{F}_2 = \vec{F}_{2a} + \vec{F}_{2m} \tag{3}$$
$$\vec{F}_3 = \vec{F}_{3a} + \vec{F}_{3m} \tag{4}$$
$$\vec{F}_4 = \vec{F}_{4a} + \vec{F}_{4m} \tag{5}$$
$$\vec{F}_5 = \vec{F}_{5a} + \vec{F}_{5m} \tag{6}$$
$$\vec{F}_6 = \vec{F}_{6a} + \vec{F}_{6m} \tag{7}$$

where $\vec{F}_{ia}$, $i = 1, 2, 3, 4, 5, 6$ denote sensing cell forces that result from an axial force, while $\vec{F}_{im}$, $i = 1, 2, 3, 4, 5, 6$ represent forces that result from bending moments.

If the sensor is subjected to an axial force $\vec{F}$ only, the force equilibrium in the z direction is expressed by

$$\sum \vec{F}_z = \vec{F} = \vec{F}_{1a} + \vec{F}_{2a} + \vec{F}_{3a} + \vec{F}_{4a} + \vec{F}_{5a} + \vec{F}_{6a}. \tag{8}$$

Moreover, the magnitude of the axial force will uniformly distribute over the sensing cells of the bottom or the top surface as shown in Fig. 3. Thus, (8) becomes

$$\begin{aligned}\vec{F} &= \vec{F}_{1a} + \vec{F}_{2a} + \vec{F}_{3a} + \vec{F}_{4a} + \vec{F}_{5a} + \vec{F}_{6a} \\ &= 3(\vec{F}_{1a} + \vec{F}_{4a}) = 3(\vec{F}_{2a} + \vec{F}_{5a}) = 3(\vec{F}_{3a} + \vec{F}_{6a}).\end{aligned} \tag{9}$$

In the presence of bending moment only, the bending moment causes the reaction forces to act on the six sensing cells. The moment can be expressed in terms of forces and radii as depicted in Fig. 3

$$\vec{M} = \sum \vec{r}_i \times \vec{F}_{im}, \qquad i = 1, 2, 3, 4, 5, 6 \tag{10}$$

where i represents the number of sensing points. Based on force equilibrium, the summation of $\vec{F}_{im}$ is zero

$$\vec{F}_{1m} + \vec{F}_{2m} + \vec{F}_{3m} + \vec{F}_{4m} + \vec{F}_{5m} + \vec{F}_{6m} = 0. \tag{11}$$

Based on (10), sensing cells can be used to detect bending moments in both x and y directions by knowing the radius and force. The radius vectors of the three sensing points are shown in Fig. 3 and are written as

$$\vec{r}_1 = \vec{r}_4 = d \cdot (1, 0, 0) \tag{12}$$
$$\vec{r}_2 = \vec{r}_5 = d \cdot \left(-\frac{1}{2}, \frac{\sqrt{3}}{2}, 0\right) \tag{13}$$
$$\vec{r}_3 = \vec{r}_6 = d \cdot \left(-\frac{1}{2}, -\frac{\sqrt{3}}{2}, 0\right) \tag{14}$$

where d is the radius. Substituting radius vectors (12)–(14) that are defined on the x–y plane into (10) leads to the moment vector as shown in Fig. 3

$$\begin{aligned}\vec{M} = \Bigg\{ & d \cdot \frac{\sqrt{3}}{2} \cdot \left[\left(\left|\vec{F}_{2m}\right| - \left|\vec{F}_{5m}\right| \right) - \left(\left|\vec{F}_{3m}\right| - \left|\vec{F}_{6m}\right| \right) \right], \\ & d \Bigg[\left(- \left|\vec{F}_{1m}\right| + \left|\vec{F}_{4m}\right| \right) + \frac{1}{2} \left(\left|\vec{F}_{2m}\right| - \left|\vec{F}_{5m}\right| \right) \\ & + \frac{1}{2} \left(\left|\vec{F}_{3m}\right| - \left|\vec{F}_{6m}\right| \right) \Bigg], 0 \Bigg\}^T.\end{aligned} \tag{15}$$

This is the moment vector expression used to calculate after measurement is carried out. From (15), the x and y components of the bending moment are respectively written as

$$M_x = d \cdot \frac{\sqrt{3}}{2} \cdot \left[\left(\left|\vec{F}_{2m}\right| - \left|\vec{F}_{5m}\right| \right) - \left(\left|\vec{F}_{3m}\right| - \left|\vec{F}_{6m}\right| \right) \right] \tag{16}$$

$$\begin{aligned}M_y = d \Bigg[& \left(- \left|\vec{F}_{1m}\right| + \left|\vec{F}_{4m}\right| \right) + \frac{1}{2} \left(\left|\vec{F}_{2m}\right| - \left|\vec{F}_{5m}\right| \right) \\ & + \frac{1}{2} \left(\left|\vec{F}_{3m}\right| - \left|\vec{F}_{6m}\right| \right) \Bigg].\end{aligned} \tag{17}$$

Force magnitudes measured on the six sensing cells are used to calculate the axial force and bending moment of rotary instruments. There may be both axial forces and bending moments applied to a sensor cell at the same time. When the force sensor is subjected to a bending moment and an axial force as depicted in Fig. 3, the force equilibrium in the z direction is expressed by

$$\begin{aligned}\sum \vec{F}_z = \vec{F} = {} & \vec{F}_{1a} + \vec{F}_{2a} + \vec{F}_{3a} + \vec{F}_{4a} + \vec{F}_{5a} + \vec{F}_{6a} + \vec{F}_{1m} \\ & + \vec{F}_{2m} + \vec{F}_{3m} + \vec{F}_{4m} + \vec{F}_{5m} + \vec{F}_{6m}.\end{aligned} \tag{18}$$

Substituting (9) and (11) into (18) leads to

$$\begin{aligned}\vec{F} &= \vec{F}_1 + \vec{F}_2 + \vec{F}_3 + \vec{F}_4 + \vec{F}_5 + \vec{F}_6 \\ &= 3(\vec{F}_{1a} + \vec{F}_{4a}) = 3(\vec{F}_{2a} + \vec{F}_{5a}) = 3(\vec{F}_{3a} + \vec{F}_{6a}).\end{aligned} \tag{19}$$

According to (19), the axial force is equal to the summation of the six forces acting on the six sensing cells. By substituting (19) into the summations of (2) and (5), (3) and (6), and (4) and (7) yield contact force sums in each of the three core regions, as shown in Fig. 3

$$\vec{F}_{1m} + \vec{F}_{4m} = (\vec{F}_1 + \vec{F}_4) - \frac{\vec{F}}{3} \tag{20}$$
$$\vec{F}_{2m} + \vec{F}_{5m} = (\vec{F}_2 + \vec{F}_5) - \frac{\vec{F}}{3} \tag{21}$$

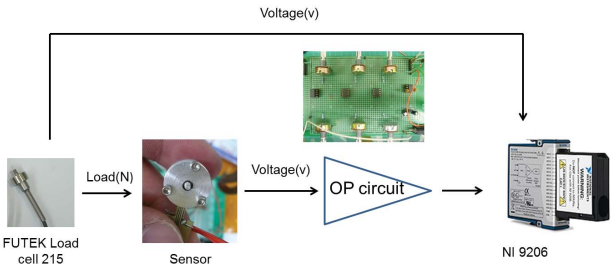

Fig. 4. Experimental setup in calibration.

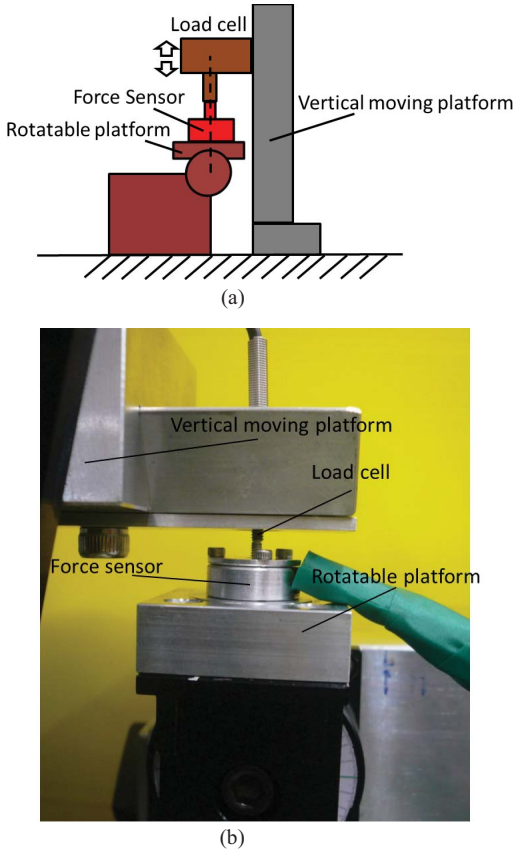

Fig. 5. (a) Schematic of the axial load experiment. (b) Equipment of the axial load experiment.

$$\vec{F}_{3m} + \vec{F}_{6m} = (\vec{F}_3 + \vec{F}_6) - \frac{\vec{F}}{3}. \tag{22}$$

In addition, x and y components of the bending moment as depicted in Fig. 3 can be calculated by substituting (20)–(22) into (16) and (17).

III. Calibration and Experiment

A. Calibration of Force Sensor

The experimental setup in the calibration is shown in Fig. 4. A vertical moving platform and a FUTEK load cell 215 are constructed to provide reference loads. The sensor generates six voltage signals, which enter an operational amplifier circuit. The six signals and the reference loads are measured and recorded by a NI 9206 DAQ card. As a result, the voltage versus load curve of the sensor is generated. Fig. 5 shows an

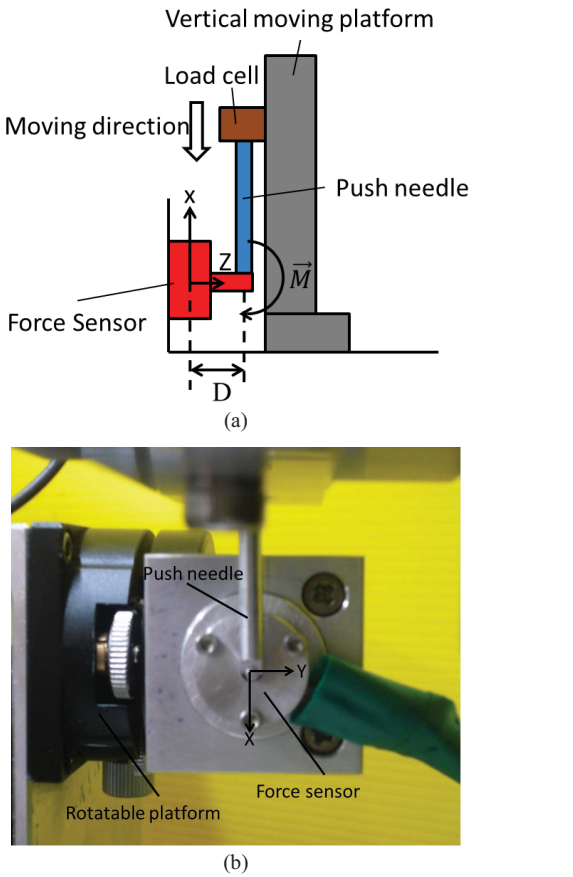

Fig. 6. (a) Schematic diagram in the bending load experiment. The push needle exerts force along the x-direction with moment arm D so as to generate moment. (b) Equipment in the bending load experiment.

axial load experimental setup. The force sensor is fixed to a rotatable platform that is adjusted to the horizontal position. The load cell is fixed to a vertical moving platform that generates and applies axial forces to the force sensor directly. Fig. 6 shows a bending load experimental setup. The rotatable platform is adjusted to the vertical position. The force sensor is fixed to the platform and contacts a push needle; therefore, the vertical moving platform can apply bending loads via the push needle to the force sensor. Fig. 7 shows an oblique load experimental setup. The force sensor is also fixed to a vertical moving platform and contacts the push needle. The rotatable platform is adjusted to make 60° with the horizontal plane; hence, the load generated by the vertical moving platform simultaneously contains both axial-component and bending-component forces.

Fig. 8(a) depicts the results of the axial downward force experiment. Sensing cells 1, 2, and 3 generate increasing voltages with load magnitudes, whereas sensing cells 4, 5, and 6 generate essentially zero voltage outputs since cells 1, 2, and 3 are located on the same plane that is subjected to the axial force. When the loading direction is downward, only those three sensing cells on the top surface in Fig. 2(b) are subjected to forces. Therefore, sensing cells 2, 3, and 4 generate output signals. Sensing cells 4, 5, and 6 do not generate voltages and hence their signal output

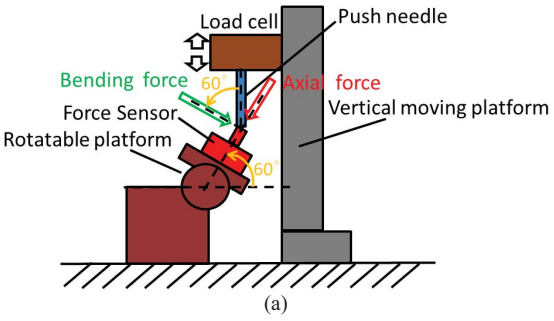

(a)

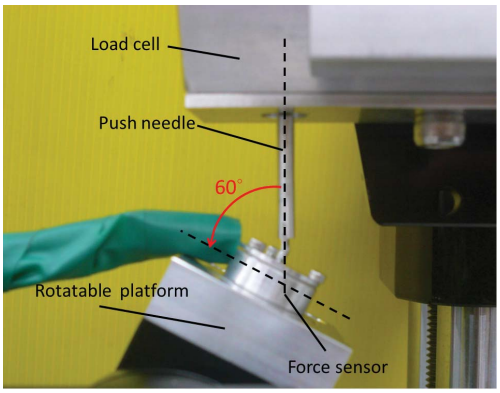

(b)

Fig. 7. Oblique load experiment: (a) schematic diagram and (b) equipment.

are close to zero. By contrast, if the loading direction is upward, only three sensing cells on the bottom surface in Fig. 2(b) are subjected to forces. Accordingly, sensing cells 4, 5, and 6 generate output signals. Fig. 8(b) shows the results of the bending load experiment. Sensing cells 1, 5, and 6 generate increasing voltages with force magnitudes, whereas sensing cells 2, 3, and 4 generate essentially zero voltage outputs due to different paste positions of sensing cells. The bending force and force arm D results in bending moment acting on the sensor. Based on Fig. 6(a), the push needle causes the y-component bending moment $\vec{M}_y$. Therefore, the x-component moment is zero and (16) can be rewritten as

$$\left|\vec{F}_{2m}\right| = \left|\vec{F}_{3m}\right|. \tag{23}$$

According to (23), the voltage magnitudes of both sensing cells 5 and 6 are the same since the position of cell 5 in Fig. 2(b) is symmetric with cell 6. In the absence of axial forces, the summation of the forces in (7) will be zero. Substituting (23) into (17) yields

$$M_y/d = \left|\vec{F}_{4m}\right| + \left|\vec{F}_{2m}\right| = \left|\vec{F}_{4m}\right| + \left|\vec{F}_{3m}\right|. \tag{24}$$

According to (24), the y-component bending moment is proportional to the difference of the forces between cells 1 and 5. Moreover, in the presence of y moment, based on Fig. 3, only sensing cells 1, 5, and 6 are subjected to forces and thus generate signal output. Fig. 8(c) shows results of a 60° oblique reference load. In this experiment, the oblique reference load generates both axial-component forces and bending-component forces on the sensor. The downward axial-component load equals the magnitude of the oblique load × sin (60°) while the bending-component load equals the magnitude of the oblique load × cos (60°). The forces applied to the sensing cells contain both the axial and the bending load simultaneously as depicted in (2)–(7). The forces caused by

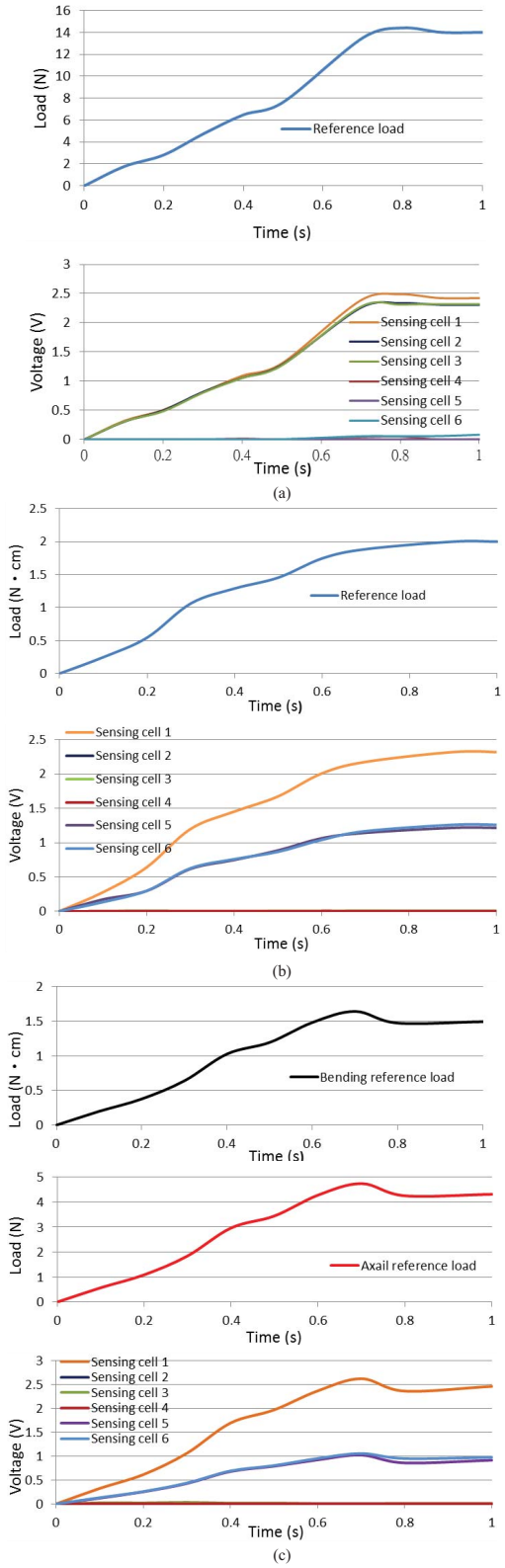

Fig. 8. Experimental results of sensor calibration. (a) Axial reference load. (b) Bending reference load. (c) 60° oblique reference load.

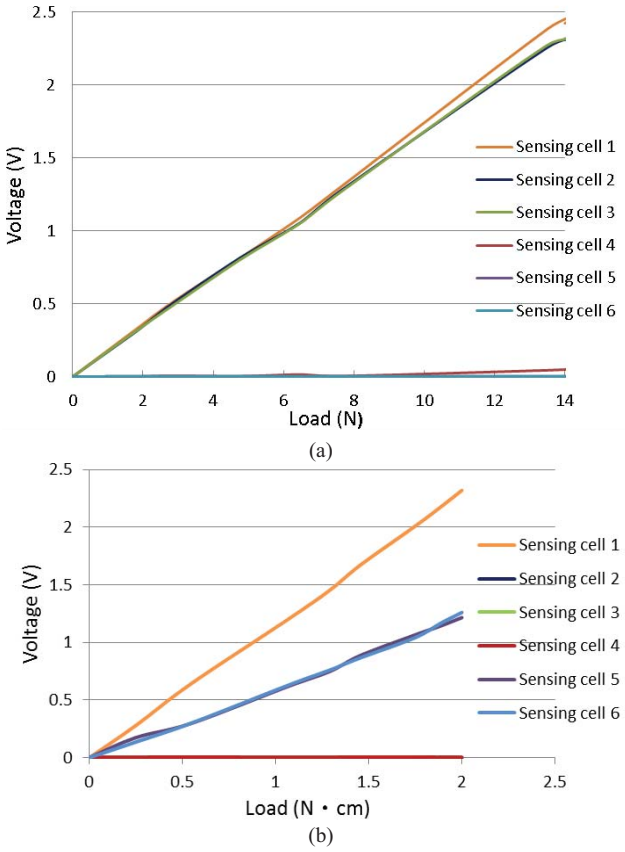

Fig. 9. Results of the relationship between voltages and loads. (a) Axial load experiment. (b) Bending load experiment.

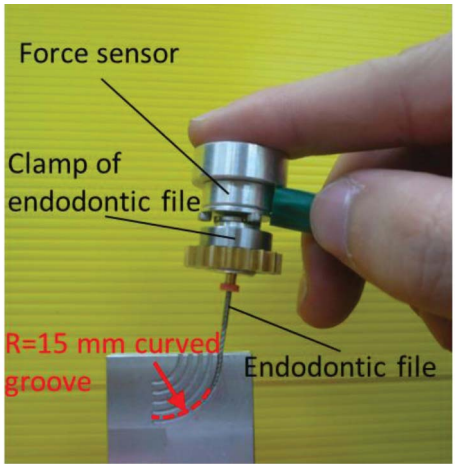

Fig. 10. Experimental setup of the endodontic instrument with the force sensor.

the axial load have the same direction as the bending load on sensing cell 1. However, the forces caused by the axial load have the opposite direction with the bending load on sensing cells 2 and 3. Accordingly, the magnitude of the cell 1 is larger than cells 2 and 3.

B. Sensor Performance

Between the load and sensor voltages, the experimental results are shown in Fig. 9, which is linear. Nonlinearities in measured axial forces and bending moments are 3.6% and

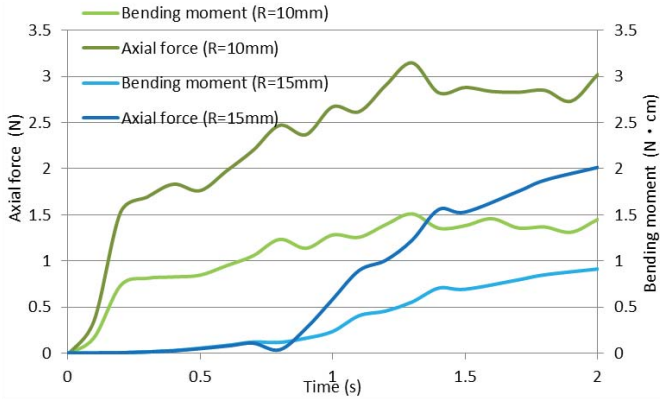

Fig. 11. Comparison of measured axial force and bending moment results between groove radii $R = 10$ and 15 mm by using the force sensor.

3.9% rate outputs, respectively. The axial force and bending moment capacities of the force sensor are about 14 N and 2 Ncm, respectively. To analyze repeatability of the sensor on the axial and the bending directions, the axial reference loads (2, 4, 6, 8, 10, 12, and 14 N) and bending reference loads (0.4, 0.6, 0.8, 1.2, 1.6, and 2 Ncm) are applied to the force sensor five times. The repeatabilities of the force sensor on the axial and bending direction are 3.1% and 3.5% rate outputs, respectively. Moreover, the sensor is tested for the hysteresis by increasing load from zero to 14 N and 2 Ncm and in turn decreasing load to zero. The hyetereses of measured axial load and bending load are calculated as 6.1% and 6.6% rate outputs, respectively. The accuracy is affected by the hysteresis.

C. Experiment

Fig. 10 depicts the experiment set up by combining the force sensor and an endodontic instrument. The force sensor is connected with the clamp of the endodontic file. Signals are recorded by a NI 9206 DAQ card and a computer. In this experiment, a K3 NiTi endodontic file with size 25 and 0.06 tapered is used and installed in the clamp. Curved grooves are used to emulate artificial canals, as depicted in Fig. 10. The file is manipulated by hand to enter the curved grooves of $R = 10$ and 15 mm radii. The length of the file that is inserted into the artificial canals is 10 mm.

Fig. 11 shows measured results by using the force sensor and an endodontic instrument. When the endodntic file is moving downward along the curved groove, it is subjected to axial force and bending moment at the same time. As time increases, the bending portion of the file increases, which enlarges axial forces and bending moments. The bending moment is inversely proportional to the radius R of artifical canals. Canals of smaller radius lead to larger axial force and bending moment. The magnitude of bending moment represents the severity of file bending. Moreover, larger bending moment increases friction force between the file and canal. And larger friction forces require the hand to exert a larger axial force to move downward the endodontic file.

IV. Conclusion

This paper has presented a miniature force sensor of diameter 14 mm and height 6 mm in order to sense both the axial

force and bending moment during endodontic therapy. The axial forces cause sensing cells on either the top or the bottom surface depicted in Fig. 2(b) to generate signal output. By contrast, when rotary instruments are subjected to a bending moment, (16) and (17) can be used to calculate the bending moment. The maximum measurable axial force and bending moment are estimated as 14 N and 2 Ncm based on 4.8 N force capacity in piezoresistive material specs, in contrast to the maximum force of 5 N for penetration applied to the instrument during endodontic therapy in practice.

The advantage of simultaneous monitoring the axial force and the bending moment lies in obtaining a complete force monitoring system used to avoid fatigue failure and surgical errors. Simultaneous sensing axial forces and bending forces can minimize the required volume of the sensor. Therefore, the proposed force sensor in this paper is feasible for sensing axial force and bending moment in endodontic treatment.

REFERENCES

[1] B. Sattapan, G. J. Nervo, J. A. Palamara, and H. H. Messer, "Defects in rotary nickel-titanium files after clinical use," *J. Endodontics*, vol. 726, no. 3, pp. 161–165, Mar. 2000.

[2] F. T. Coutinho, R. L. Krebs, T. C. Berlinck, and R. G. Galindo, "Retrieval of a broken endodontic instrument using cyanoacrylate adhesive: Case report," *J. Braz Dent*, vol. 9, no. 1, pp. 57–60, 1998.

[3] X. Wei, J. Ling, J. Jiang, X. Huang, and L. Liu, "Modes of failure of ProTaper nickel–titanium rotary instruments after clinical use," *J. Endodontics*, vol. 33, no. 3, pp. 276–279, Mar. 2007.

[4] G. Plotino, N. M. Grande, M. Cordaro, L. Testarelli, and G. Gambarini, "A review of cyclic fatigue testing of nickel-titanium rotary instruments," *J. Endodontics*, vol. 35, no. 11, pp. 1469–1476, Nov. 2009.

[5] J. P. Oruett, D. J. Clement, and D. L. Carnes, "Cyclic fatigue testing of nickel-titanium endodontic instruments," *J. Endodontics*, vol. 23, no. 2, pp. 77–86, Feb. 1997.

[6] O. A. Peters, A. Laib, P. Ruegsegger, and F. Barbakow, "Three-dimensional analysis of root canal geometry by high-resolution computed tomography," *J. Dental Res.*, vol. 79, no. 6, pp. 1405–1409, 2000.

[7] C. S. Shin and M. W. Lin, "An optical fiber-based curvature sensor for endodontic files inside a tooth root canal," *IEEE Sensors J.*, vol. 10, no. 6, pp. 1061–1065, Jun. 2010.

[8] O. A. Peters and F. Barbakow, "Dynamic torque and apical forces of ProFile. 04 rotary instruments during preparation of curved canals," *Int. Endodontics J.*, vol. 35, no. 4, pp. 379–389, Apr. 2002.

[9] A. P. Boresi and R. J. Schmidt "Fatigue: Progressive fracture," in *Advanced Mechanic of Materials*, 6th ed. New York, NY, USA: Wiley, 2003, pp. 567–584.

[10] R. Liu, Y. L. Kwok, Y. Li, T. T. H. Lao, X. Zhang, and X. Q. Dai, "Objective evaluation of skin pressure distribution of graduated elastic compression stockings," *Dermatol. Surgery*, vol. 31, no. 6, pp. 615–624, 2005.

[11] E. S. Hwang, Y. R. Yoon, H. R. Yoon, T. M. Shin, and Y. J. Kim, "Flexible contact force sensing device using metal/polymer multilayer structure for robotic applications," *Sens. Mater.*, vol. 20, no. 2, pp. 55–69, 2008.

[12] T. Liu, Y. Inoue, and K. Shibata, "A small and low-cost 3-D tactile sensor for a wearable force plate," *IEEE Sensors J.*, vol. 9, no. 9, pp. 1061–1065, Sep. 2009.

[13] Interlink Electronics Inc. (2010, Oct.). *Interlink Electronics FSR Force Sensing Resistors*, Camarillo, CA, USA [Online]. Available: http://www.digikey.com/Web%20Export/Supplier%20Content/Interlink Electronics_1027/PDF/Interlink_Electronics_Integration_Guide.pdf?redirected=1

Chih-Chiang Tsao was born in Taiwan in 1986. He received the B.S. degree in mechanical and electromechanical engineering from National Sun Yat-sen University, Kaohsiung, Taiwan, in 2008.

He is currently pursuing the Ph.D. degree in mechanical engineering at National Chiao Tung University, Hsinchu, Taiwan. His research interests are focused on force sensors, piezoelectric transducers, and endodontic instrument mechanical analysis.

Fang-Yu Lin received the B.S. and M.S. degrees in mechanical engineering from National Chiao Tung University, Hsinchu, Taiwan, in 2009 and 2010, respectively. He is currently a Research Assistant with the Department of Electrical Engineering, National Taiwan University, Taipei, Taiwan. His current research interests include endodontic therapy assistant system, medical and rehabilitation robots.

Ji-Wei Liou received the M.S. degree from National Taiwan University, Taipei, Taiwan. He is currently a Professor with the Department of Dentistry, Division of Endodontics, Mackay Memorial Hospital, Taipei, Taiwan. His current research interests include Ni-Ti instruments on dental clinical practice.

Ping-Han Wen received the M.D.Sc. degree in endodontics from National Taiwan University, Taipei, Taiwan, in 2003. He was certified as an Endodontist by the Academy of Endodontology, Taiwan, in 2009. He was a Visiting Staff Member at the Dental Department, Mackay Memorial Hospital, Taipei, from 2009 to 2012. He is currently an Endodontist at Chengan Dental Clinic, Taipei.

Chieh-Chung Peng received the Doctor of Dental Surgery (D.D.S.) degree from Kaohsiung Medical University, Kaohsiung, Taiwan, in 2008. After graduation, he received Endodontic special training at Mackay Memorial Hospital, Taipei, Taiwan, from 2009 to 2012. He is currently a Visiting Staff Member at the Dental Department, Mackay Memorial Hospital, Taipei.

Tzong-Shi Liu received the B.S. degree from National Taiwan University, Taipei, Taiwan, in 1979, and the M.S. and Ph.D. degrees from the University of Iowa, Iowa, IA, USA, in 1982 and 1986, respectively, all in mechanical engineering. He has been teaching in National Chiao Tung University, Hsinchu, Taiwan, since 1987. His research interests include robotics, electric motor, mechatronics, and automatic control.